Microstructure and local mechanical properties of pea starch / protein composites

Imen Jebalia, Magdalena Kristiawan, Maria Charalambides, Samuel A. Humphry-Baker, Guy Della Valle, Sofiane Guessasma

Composites Part C: Open Access 8 (2022) 100272

Contents lists available at ScienceDirect

Composites Part C: Open Access

journal homepage: www.sciencedirect.com/journal/composites-part-c-open-access

Microstructure and local mechanical properties of pea starch / protein composites

I. Jebalia [a], M. Kristiawan [a], M.N. Charalambides [b], S. Humphry-Baker [c], G.Della Valle [a], S. Guessasma [a,*]

[a] INRAE, UR 1268 Biopolymers Interactions and Assemblies (BIA), 44316 Nantes, France
[b] Department of Mechanical Engineering, Imperial College London, London SW7 2AZ, UK
[c] Department of Materials, Imperial College London, London, SW7 2BP, UK

ARTICLE INFO

Keywords:
Nanoindentation
Young's modulus
Image analysis
Interphase
Morphology

ABSTRACT

Biopolymer composites based on pea starch-protein blends and pea flour are processed using extrusion at various levels of specific mechanical energy (*SME*). Their morphology was a continuous matrix phase of starch with embedded protein particles, as revealed by Confocal Laser Scanning Microscopy (CLSM). The motivation is to correlate the local Young's modulus (*E*) in starch and protein phases, as well as their interphase, through nanoindentation tests to macroscopic three-point bending testing results of starch-protein composites. The differences between *E* of starch and protein phases and interphase were significant and their values were found to vary in the ranges of 4.2–7, 3–6.9 and 4–6.9 GPa, respectively. The local *E* can be tuned by the protein content and composite morphology, the latter depending on the level of transformation of the biopolymers during extrusion (*SME*). Pea flour composites have larger modulus values, which can be attributed to the presence of fibres.

Abbreviations

A	total area of protein aggregates (mm^2)
A_c	projected contact area between sample and indenter (μm^2)
A_{Ref}	protein aggregates total area of a reference sample
AFP	area fraction of protein phase (%)
CLSM	confocal laser scanning microscopy
d	indent width
D	indents spacing
D_{50}	median protein aggregates width (μm)
db	dry basis
E_i	Young's modulus of the indenter (GPa)
E_r	reduced modulus (GPa)
E	Young's modulus (GPa)
F	force (N)
H	high level of specific mechanical energy
h	indentation depth (μm)
h_c	contact depth (μm)
h_{max}	maximum depth (μm)
I_i	interface index
L	low level of specific mechanical energy
MC	moisture content (wb)
N	screw speed (rpm)
P	total perimeter of protein aggregates (mm)
P_{Ref}	protein aggregates total perimeter of a reference sample
PPI	pea protein isolate
PF	pea flour
RH	relative humidity (%)
S	contact stiffness
SP blend	starch-protein blend
S/P	starch/protein interphase
P/P	protein/protein interphase
S/F	starch/fibre interphase
SME	specific mechanical energy (kJ/kg)
T	temperature of the last barrel of the extruder (°C)
wb	wet basis
ν	Poisson's coefficient of the specimen
ν_i	Poisson's coefficient of the indenter

* Corresponding author.
E-mail addresses: imen.jebalia@inrae.fr (I. Jebalia), magdalena.kristiawan@inrae.fr (M. Kristiawan), m.charalambides@imperial.ac.uk (M.N. Charalambides), s.humphry-baker@imperial.ac.uk (S. Humphry-Baker), guy.della-valle@inrae.fr (G.Della Valle), sofiane.guessasma@inrae.fr (S. Guessasma).

https://doi.org/10.1016/j.jcomc.2022.100272

Available online 2 May 2022

1. Introduction

In recent years, there has been a growing interest in developing biopolymer-based composites, which can replace fossil fuel and petroleum-based products in many applications. This trend leads to new agricultural, environmental, manufacturing, and consumer benefits [1]. Widespread materials based on renewable resources have been designed for nonfood applications. They include cellulosic plastics, polylactides (PLA), starch plastics, and soy-based plastics [1]. Considerable research has been performed on starch-based materials due to their versatility, inexpensive price, abundance, and biodegradability [2]. However, a few of their drawbacks need to be overcome, such as their sensitivity to moisture and inferior mechanical properties as compared to synthetic polymers [3, 4]. To overcome these limitations and therefore be competitive with synthetic composites, starch has been blended with other biopolymers such as chitosan [5], polylactide [6], rice husk biochar [7], and different natural ligno-cellulosic fibres [8–10]. Indeed, the incorporation of fibre in starch matrix has proven to be an effective method in obtaining high-performance starch-based composite materials [5, 11, 12]. In all cases, the blending of biopolymers to produce composite materials requires special attention to the filler-matrix interface issue [13, 14] because only a well-adhered interface allows full stress transfer from the matrix to the filler. In this paper, composites composed of starch and protein from pea are addressed for the first time. Starch-protein composites have potential applications in various fields, e.g. biomedical such as drug delivery, tissue regeneration, scaffolds [15, 16] and protein fortified foods [17]. Both potential food and non-food applications of these composites are provided as a supplementary table (Table A1). In case of airy foods (i.e. solid food foams), the structure of wall material can be considered as a composite with dispersed protein particles within a continuous starchy matrix [18]. The main structural changes that occur during processing at high temperature and shear involve starch melting and depolymerization [19], protein denaturation and aggregation [17]. As processing intensity increases, the starch becomes more amorphous and disordered, whereas proteins order in large hydrophobic aggregates. In turn, these changes influence the composite morphology and mechanical properties, which opens the prospect for the design of starch-protein composites with targeted properties. The global mechanical properties of starchy composites are obtained from testing on universal testing machines where the extracted engineering constants such Young's modulus or mechanical strength are indirectly related to the phase content through the overall composition. The global mechanical properties of starchy composites can take lower values compared to intrinsic properties of the phases [33] or can be in the same range of values. These mechanical properties depend on the processing conditions such as the plasticizer content (glycerol, water) and the starch/protein mixture composition. In addition to plasticizer effect, samples composition, and interfaces considered in the starchy composites, protein cross-linking also plays a critical role in determining their macroscopic mechanical properties such as tensile fracture strength, commonly seen in protein derived bioplastics. For instance, Young's moduli of corn composites are found to vary in the range of 0.5–3.2 GPa for moisture content 12% and 22% [33]. Generally speaking, protein addition has a negative effect on the global mechanical properties of composites, which has been attributed to poor adhesion between the constituents. Moreover, it has been evidenced that the global mechanical properties of starch-protein composites depend on their morphological features, mainly the starch-protein interface index, defined as the ratio of the aggregate perimeter to the square root of the total aggregates area [30]. Local mechanical properties of starchy composites are obtained using specific equipment such as Atomic Force Microscopy (AFM) or nanoindentation, which allow sensing the material response at the microstructural scale. Some deviation between the global and local properties can be obtained depending on the nature of the phase arrangement and the quality of the interface. This is, for instance, the case for the starch-protein composites [30], where composites may present different local mechanical properties in starch and proteins phases as well as in the interface. To quantify the local mechanical response of composite materials, local mechanical testing can be used such as the nanoindentation test [20]. This technique is capable of measuring local engineering constants of biopolymers, such as hardness and stiffness at the micron-scale [21–24]. Nanoindentation studies can determine the effect of the reinforcement on the biocomposite mechanical behaviour [12] and evaluate the composite's interphases properties [25]. However, local mechanical properties of starch-protein composites have scarcely been measured by this technique [26–28]. Furthermore, literature studies have focused on cereal based composites with a limited range of protein content, aggregation level and morphology, due to the low content of protein in cereals (<15%, dry basis db). To push forward the potential of starch-protein composites, it is necessary to study their local mechanical properties over a wider range of protein compositions, a purpose for which pulses (e.g. pea, lentil, faba bean) with higher protein content (up to ~40% db) are well suited. Furthermore, pulses have mainly been used for food and feed and not been exploited to design biocomposites. In a previous study, the overall mechanical properties of pea composites with starch/protein ratio of 2 were related to microstructural features such as interface index based on confocal microscopy [30]. The study concluded that weak starch-protein imperfect interface would explain the tendencies observed especially the presence of voids between the starchy matrix and the protein aggregates. In a previous study by the research group [29], the impact of extrusion variables (temperature, specific mechanical energy) of pea flour (protein 24% d.b.) was studied on the structural modification of starch and protein, expressed in terms of starch and protein solubility and foaming density. In another study by the authors [30], the impact of morphological features was addressed on the global mechanical properties of one type of pea starch – protein composite made of 24% db of extruded pea flour. In this paper, we aim to determine accurately the local mechanical properties of each phase (starch, protein) in pea composites using a larger domain of protein content, and to elucidate the role of the interphase and starch-protein morphology on composite texture. In this purpose, we have combined the use of confocal scanning laser microscopy (CSLM) and nanoindentation tools to establish the relationship between bio-composites microstructure and local mechanical properties. The main hypothesis investigated in this work is that the protein – starch interface plays an important role in controlling the mechanical properties of the composite, which are essential to consider the use of these composites in engineering applications.

2. Materials & methods

2.1. Materials

Native pea flour (PF), starch-protein (SP) blends, pea starch (S) and pea protein isolates (PPI) were used in this study. Yellow pea grits (Pisum Sativum L.) were purchased from Sotexpro (France) and ground (SARL Giraud, France) in order to obtain pea flour. Pea starch (amylose content: 35%) and pea protein isolate (Nutralys® F85 F) were supplied by Roquettes Frères S.A. (Lestrem, France). The median diameter of PF , S and PPI determined by laser diffraction (Partica LA-960, HORIBA, Japan) was 480, 27 and 72 μm, respectively.

The chemical composition of the raw materials determined by standard enzymatic and Kjeldahl methods, described in detail elsewhere [29], are presented in Table 1. SP Blends with starch/protein ratio 2/1, 1/1 and 1/2 (weight/weight, db) were obtained by mixing pea starch and PPI using a Kenwood mixer. Note that PF had an S/P ratio of 1.92, which is close to that of the SP 2/1 blend.

2.2. Materials processing

The materials (PF, SP blends, S, PPI) were extruded as dense strips

Table 1
Chemical composition of raw material (% db).

Raw material	Proteins	Starch	Ash	Lipid	Others**
Pea starch (S)	0.5	98	0.1	-	1.4
Pea flour (PF)	24	46	2	2	26
SP* blend 2/1	32	63	2	-	3
SP* blend 1/1	46	47	2	-	5
SP* blend 1/2	61	31	3	-	5
Pea protein isolates (PPI)	88	0.4	4	-	7.6

* SP: starch-protein.
** Fibre and other components, determined by difference method [27,37].

using a laboratory scale co-rotating twin-screw extruder (Thermo Scientific™ Process 11, Germany) equipped with a plate die (section: 26 × 1 mm^2; length: 70 mm). The extruder configuration and operating conditions have been described in a previous work (Fig. 1) [30]. In order to obtain composites with a wide range of starch-protein morphological features and mechanical properties, each raw material was extruded at two levels of specific mechanical energy (*SME):* low (*L*, 100–1000 kJ/kg) and high (*H,* 1000–2000 kJ/kg), as indicated in Table 2, by modifying moisture content *MC* (25–35% wb), screw rotation speed *N* (150–700 rpm) and temperature of the last barrel of the extruder *T* (90–150 °C). The samples selected for this study are those covering the widest range of Young's modulus measured at the global scale (flexural test) and interface index. In this study, the SME level is used as a relevant extrusion variable to rank the studied materials according to the intensity of processing, and thus of structural changes, for a single formulation. Immediately after extrusion, the dense ribbons were dried at 40 °C for 24 h in order to avoid starch retrogradation and to obtain a final *MC* of less than 10% wb (Fig. 1).

Hereafter, the sample names indicate the *SME* level (*L, H*), the formulation (*PF*: pea flour, *SP*: starch-protein blend) and starch/protein ratio (2/1, 1/1, 1/2) in the case of blends. The samples names and corresponding properties were given in Table 2.

2.3. Microstructure observation & image analysis

The microstructure of pea composites was observed using confocal laser scanning microscopy (CLSM) (Nikon A1) with an attached NIS imaging system (Nikon, Germany) and quantified by image analysis.

Before cryo-sectioning, the composites were hydrated by conditioning at 20 °C and ambient relative humidity (RH) of 98% for 4 days to avoid specimen cracking while cutting. it has been checked that this conditioning time does not induce any structural change. For protein labelling, one-part (by mass) of 0.01% (volume/volume) fuchsine acid in 1% (volume/volume) acetic acid was mixed with one part of Kaiser's glycerol/gelatine solution, which was melted at 40 °C. The specimen slices (thickness: 20 μm) were obtained by cutting the embedded sample within the freezing medium tissue (FMT, Tissue-Tek O.C.T) perpendicularly to the extrusion flow using a cryotome at −20 °C. FMT was used to

Table 2
The extrusion specific mechanical energy (*SME*) and morphological features of pea composites.

Raw material	Samples code	Protein content (%, db)	*SME* (kJ/kg)	I_i	D_{50} (μm)	*AFP* (%)
PPI	PPI	88	95	–	–	–
Pea starch	S	0.5	500	–	–	–
Pea flour	L_PF	24	1149	1.9 ± 0.2	22 ± 3	24±4
	H_PF		1952	2.4 ± 0.1	15 ± 2	20±2
SP blend 2/1	L_SP2/1	32	992	1 ± 0.04	40 ± 4	25±4
	H_SP2/1		1981	1.1 ± 0.04	27 ± 4	17±5
SP blend 1/1	L_SP1/1	46	141	1 ± 0.1	29 ± 4	56±8
	H_SP1/1		905	1.7 ± 0.2	19 ± 3	44±9
SP blend 1/2	L_SP1/2	61	511	1.3 ± 0.3	47 ± 7	50±5
	H_SP1/2		1077	0.9 ± 0.1	56 ± 8	34 ±10

PPI: pea protein isolates, S: pea starch, L: low *SME*; H: high *SME*, PF: pea flour, SP: starch-protein blend, I_i: interface index, D_{50}: median width of protein aggregates, *AFP*: area fraction of protein phase.

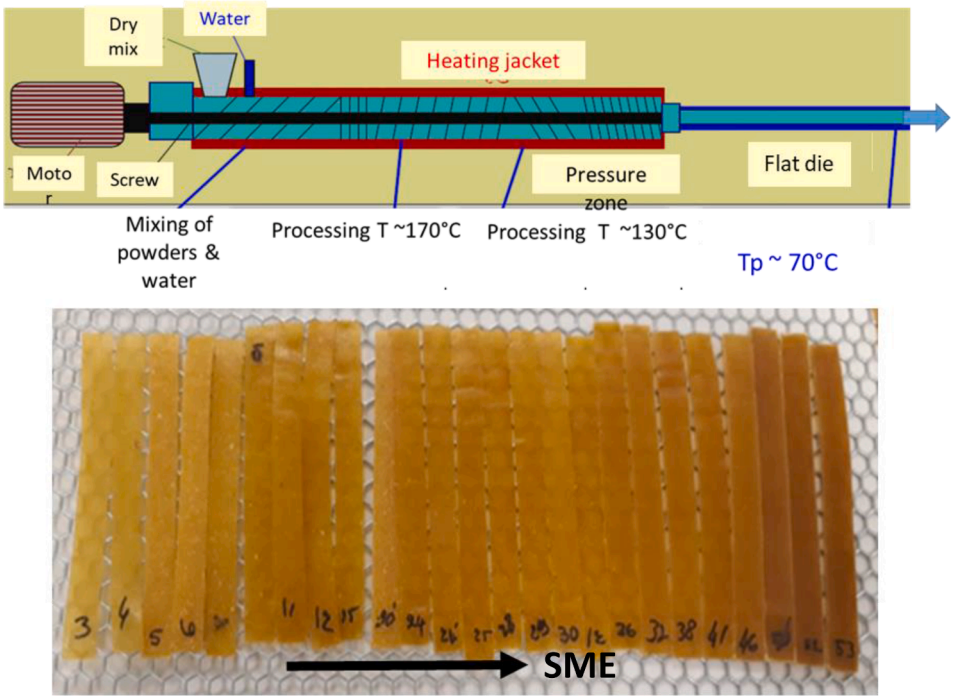

Fig. 1. Typical extrusion process used to obtain starchy composites with varied SME.

support sections during cryotomy and to reduce curling, allowing easier handling of flat serial sections. Then, the slices were mounted in the frozen state onto microscope slides, covered with stained Kaiser's solution and a glass coverslip. Kaiser's solution was used to improve the adhesion of specimen slices on microscope slides and to maintain microstructure. This solution solidifies rapidly after dropping on the slide allowing the best maintain of microstructure. The slides were stored for 24 h at room temperature to be dried and to ensure optimum diffusion of the markers.

Samples were examined in the epifluorescence mode of the microscope, excited by a green laser beam at 561 nm. The emitted light was selected by a long-pass filter at 570–620 nm. Images of 512 × 512 pixels were taken with a resolution of 1.24 μm/pixel. A Matlab® program was implemented to obtain binary images from the CLSM images which were digitized by applying a grey level threshold following a k-mean algorithm [31]. Each finite particle in the image was labelled. From the labelled images, the following features were determined: area fraction of protein phase (*AFP*,%), median particle width (D_{50}, μm), total area (*A*, mm^2) and total perimeter (*P*, mm) of protein aggregates. The starch-protein interface index (I_i, dimensionless) was then computed as follows [27]:

$$I_i = \left(P / P_{Ref}\right) \Big/ \sqrt{A/A_{Ref}} \tag{1}$$

where P_{Ref} and A_{Ref} are respectively the protein aggregates' total perimeter and total area of a reference sample L_SP1/1. This composite has been chosen as a reference because it has the largest value of protein aggregates total area, likely because it was extruded at lowest *SME* (Table 2), which largely balanced its lower protein content than L_SP1/2, as explained in more detail in results section. The variation of the digitization threshold (± 10%) induced an uncertainty in the particle area and perimeter values of about 10%.

A distribution of the protein particles cumulative area was then built and fitted by the Gompertz function [32]:

$$y = c \times exp^{(-\exp(-k(x-x_c)))} \tag{2}$$

where *y* is the cumulative area of particles having a width less than or equal to the width *x*, *c* is the amplitude of the cumulative area (=100), x_c is the abscissa of the inflection point and *k* is the slope of the curve at this point, hence describing the particle width uniformity. D_{50} was computed from the Gompertz fit at *y* = 50% of the cumulated area.

2.4. Three-point bending trials

The global mechanical properties of specimen strips (t_h × 100 × 10 mm^3) were determined by a three-point bending test mounted on a dynamometer (Adamel Lhomargy, France) following the ASTM D790 norm. Although, the bending test is a heterogenous test where both compression and tension stresses develop, the engineering stiffness derived from this test can be compared to the inherent stiffness of the composite assuming that Young's modulus is the same when measured under compression or tension. The thickness (t_h) of specimens was measured at three locations with a Vernier calliper. The support span (L) was 40 mm and the crosshead speed was 100 mm/min. The tests were performed until the specimen fractured. Engineering stress σ (Pa) – strain ε (%) curve was derived from the force–crosshead displacement data as follows:

$$\sigma = \frac{3FL}{2ht_h^2} \tag{3}$$

$$\varepsilon = \frac{6dt_h}{L^2} \tag{4}$$

where F is the force (N), h is the specimen width (0.01 m) and d is the crosshead displacement (m). The engineering flexural modulus E (GPa) was measured as the slope of the linear part of the engineering stress - strain curve. The measurements of mechanical properties were performed ten times per condition, leading to an average variability of 20%.

2.5. Nanoindentation experiments

The nanoindentation protocol was adapted to the studied materials including fixing method, depth and grid indentation. Samples approximately 3 mm in height were prepared for nanoindentation experiments using a microtome modular system equipped with a glass knife to obtain a flat and smooth surface. Because of the sensitivity of starch composites to humidity, samples were stored in a desiccator at stable relative humidity (NaBr, RH = 59% at 20 °C) to obtain a uniform moisture distribution prior to mechanical testing (12±0.5% wb). This moisture content was controlled by measuring the dry matter (after 2 h of heating at 130 °C). The samples (≈ 5 × 1 mm^2 in cross section) were glued onto a cylindrical holder using an acrylic mounting system at least one hour prior to the test.

Indentations were performed using a NanoTest Vantage apparatus from Micro Mechanics (Wrexham, U.K.) at room environment (RH = 22% at 23 °C). A three-sided pyramid (Berkovich) diamond indenter was used (Fig. 2). The force was increased at 1 mN/s until a maximum load was reached, followed by a 60 s hold, and then unloaded at the same rate. The final moisture content of samples measured prior testing was of 8 + 1%.

To minimize the indentation size effect, the variation of Young's modulus (*E*) as a function of indentation depth was evaluated for extruded pure pea starch (S), PPI, and H_PF composite.

An indent spacing, *D*, of 75 μm (at least three times the indent width, *d*, was set up in a grid of 25 indents (5 × 5). Indents were observed using an optical microscope attached to the nanoindenter, allowing the phase-location of each indent to be identified (Fig. 2). Indents are considered to be in the interphase if they overlap both phases.

The value of *E* was determined using the Oliver and Pharr method [20]. *E* was computed from the reduced modulus E_r which accounts for the deformation of both the indenter and the sample as follows:

$$1/E_r = \left(1-\nu^2\right)/E + \left(1-\nu_i^2\right)/E_i \tag{5}$$

where E_i and ν_i refer to the Young's modulus and Poisson's coefficient of the indenter (1141 GPa and 0.07, respectively [20]). *E* and ν are the values corresponding to the specimen. The reduced modulus E_r of the specimen was determined from the contact stiffness (*S*) which, is measured as the slope of the tangent line to the unloading curve at the maximum loading point. The tip geometry calibration was performed using a series of 100 indentation tests on fused silica (reference material) at a series of loads from 0.5mN to 200 mN.

2.6. Statistical analysis

ANOVA analysis followed by the Fisher's least significant difference test was carried out to study both the significant difference in modulus between phases for the same sample, and also between composites of different compositions and levels of transformation. The analysis was performed using Microsoft Xlstat software 2020 (Addinsoft, Paris, France).

3. Results

3.1. Analysis of composite microstructure

The CSLM images shown in Fig. 3 suggest that the microstructure of pea composites consisted of protein aggregates (particles) dispersed in a continuous matrix of amorphous starch, regardless of the composition and processing conditions.

Similar composite morphology was also observed in previous studies

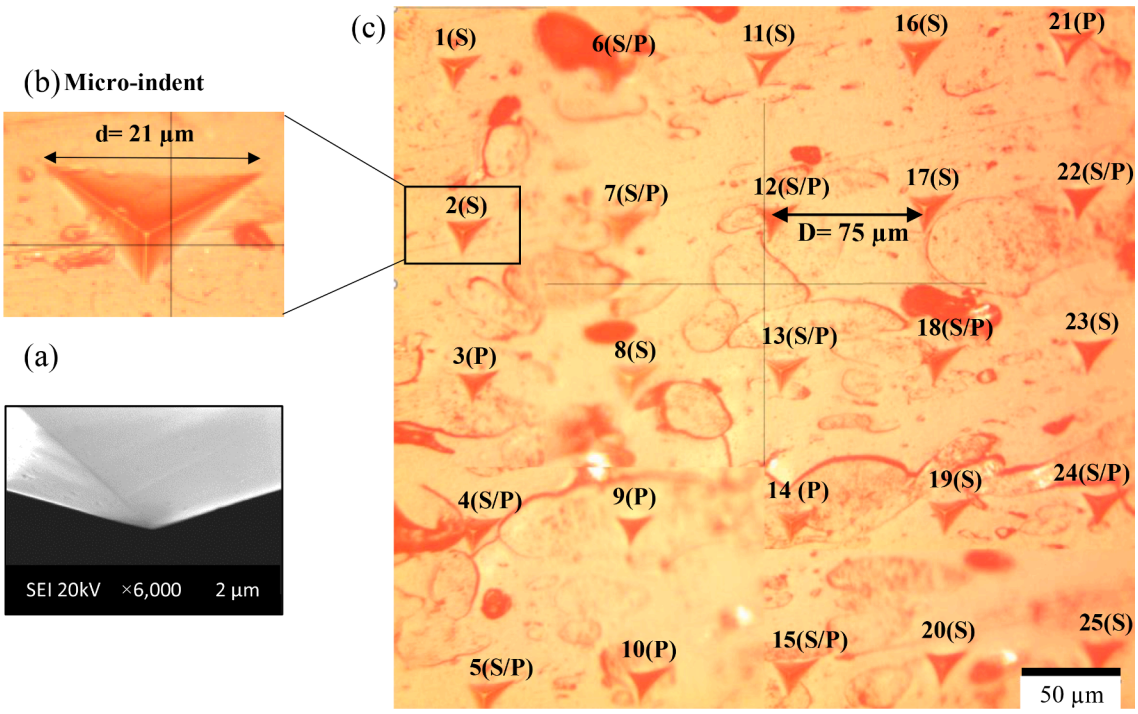

Fig. 2. Presentation of a snapshot of a microindent (a), a picture of the Berkovich indenter tip taken by Scanning Electron Microscopy (b) and a micrograph of a microindent grid performed on a pea composite (H_SP2/1) The indent width (*d*) was 21 µm which is seven times higher than the indentation depth (3 µm). (c). The grid arrangement was 5 lines × 5 columns with a spacing (D) of 75 µm between adjacent indents.

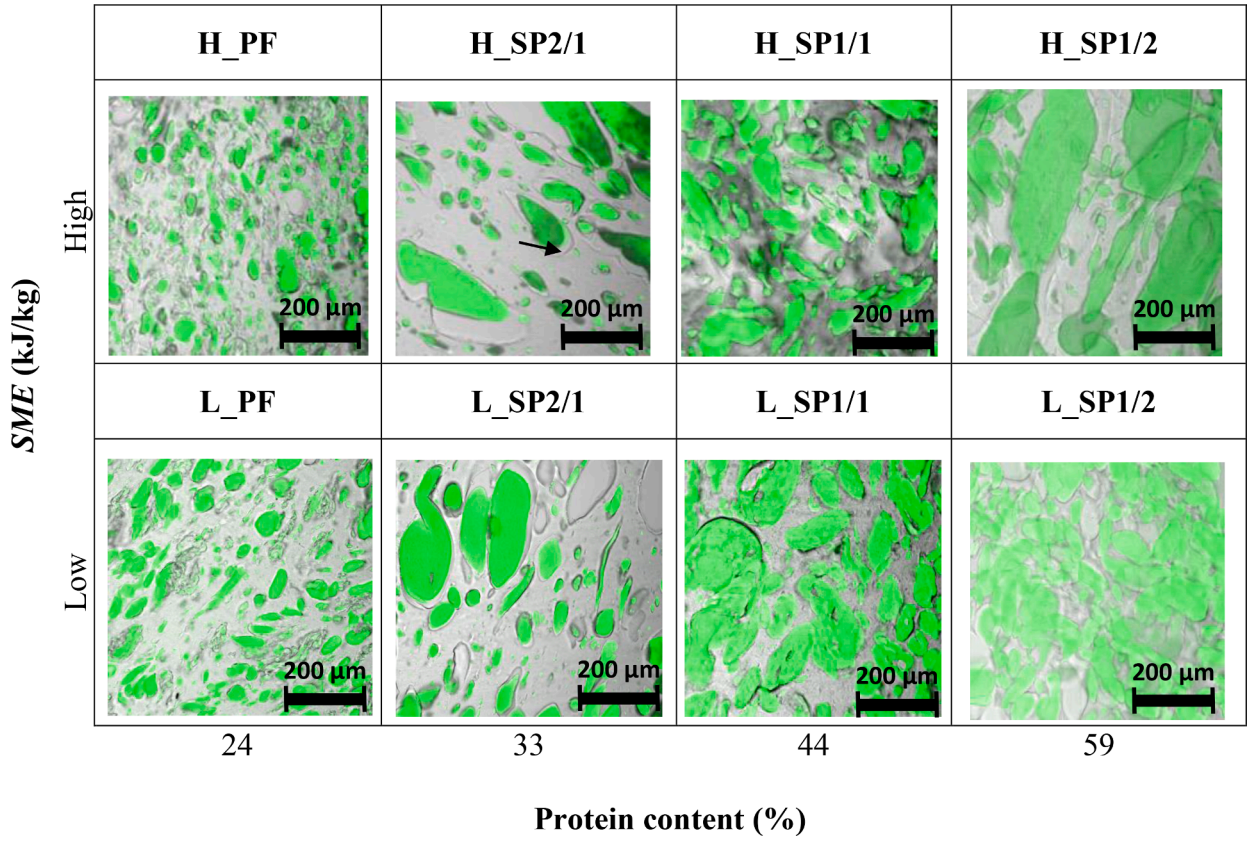

Fig. 3. CLSM images of pea composites showing the effect of protein content and specific mechanical energy *SME* on morphology (PF: pea flour, SP: starch/protein blends obtained at low (*L*) and high (H) levels of *SME*), observed by CLSM. The proteins are stained green (darker when printed in greyscale) with fuchsin acid. Unstained amorphous starch is presented in grey. Some grey spaces surrounding the aggregates and delimited with grey lines indicate voids at the interface of starch and protein aggregates, marked by arrows. While voids can be a triggering effect for stress localization and crack initiation, the effect of voids in the present study is not evaluated as the main concern is to evaluate the variation of phase and interface elastic properties.

for starch-zein blends [33, 34]. Some voids were observed at the interface of starch and protein phases. These voids can result from interfacial debonding during cooling on exit from the extruder die, or from sample cryo-sectioning for microscopy analysis, as already observed for starch-zein blends [33, 34]. In fact, during cooling, the samples are dried, which can lead to shrinkage of starch and protein phases. At the die exit, the rubbery product undergoes simultaneous heat and mass transfer, i.e. cooling and water evaporation, until its temperature crossed its glass transition temperature and the structure is set. During drying, occurring within a few seconds, the product experiences shrinkage and therefore, interfacial debonding can possible occur due to lack of starch/protein compatibility.

The large domains of extrusion variables (*SME* 140 – 1950 kJ/kg) and composition lead to different morphologies and microstructural features, in terms of I_i (0.9–2.4), D_{50} (15–56 μm) and *AFP* (17–56%) (Table 2). For the same compositions, *AFP* decreases with increasing *SME* values, which is likely due to the starch becoming more disordered and the protein more aggregated, as explained in the introduction and discussed in earlier work [30]. In a standard compounding process, the increased energy should help to disperse the phases. However, proteins do not behave as a standard polymeric material [35]. The reason for the high aggregation when protein content is high can be captured from the abundant interactions between proteins, including mainly the linkage by disulphide bonds, which form aggregates. From the processing viewpoint, the two factors that drives the decrease of the agglomeration tendency is the protein content (L_PF) and the SME value (H_SP1/1). The observed structural changes also explain why, L_SP1/1 has larger *AFP* than SP1/2, for instance. The distributions of the protein particles

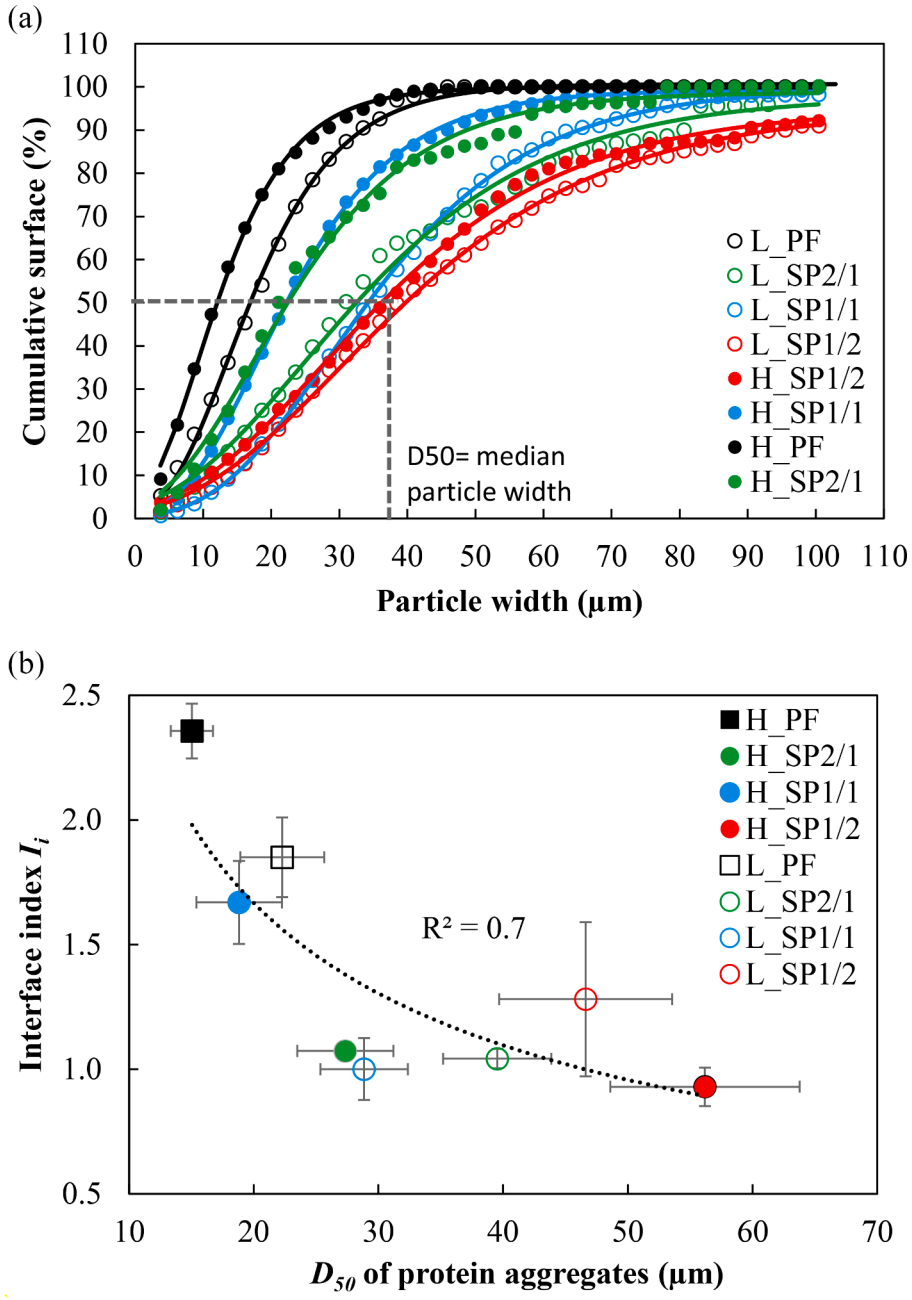

Fig. 4. (a) Cumulative distribution of protein aggregate width for pea composites, solid lines represent data fitting using the Gompertz function (Eq. (2), $R^2 > 0.98$) and (b) variation of starch/protein interface index (I_i) with median width of protein aggregates (D_{50}) determined by CSLM images analysis. Empty and full symbols refer to samples extruded at low and high *SME,* respectively. The dotted line in (b) represent the best data fitting, according to the function $y = 10.2\,x^{-0.6}$ ($R^2 = 0.7$).

cumulative area are depicted in Fig. 4a.

The successful curve fitting by the Gompertz function (Eq. (2)) allowed the accurate determination of the D_{50}. For the same S/P ratio, SP 2/1 blends presented larger protein aggregates (D_{50} = 27–40 μm) than PF composites (D_{50} = 15–22 μm), which could be due to the increased fibre content in the case of pea flour [30].

The analysis of the CSLM images showed a negative correlation (R^2=0.7) betweenD_{50} and I_i) (Fig. 4b). Therefore, considering all samples, irrespective of their composition and *SME* level, the general trend suggests that the larger the particles, the smaller the interface. This statement is confirmed by the qualitative trend observed from CLSM images (Fig. 3): many small protein aggregates (L_PF) lead to a larger total perimeter than a few large and sparse aggregates (H_SP2/1). The dispersion of data is due to the irregular shapes of particles, as suggested by the CLSM micrographs in Fig. 3.

3.2. Nanoindentation results

Fig. 5a exhibits the sensitivity of extruded S , PPI and H_PF composite stiffness to the indentation depth. The moduli are stable at depths greater than 3 μm, but rises steeply at smaller depths. The large increase in modulus for depths smaller than 3 μm is partly due to the indentation size effect. It is also related to the difficulty of correctly measuring the contact surface due to the residual roughness of the specimen. Thus, in all subsequent experiments, an indent depth of 3 μm was used, corresponding to a width, *d*, of ~ 21 μm (see Fig. 5). Fig. 5b shows a comparison of *E* of fused silica reference computed using the perfectly sharp tip assumption, and the tip-shape correction. For validation, the computed *E* was compared to the one found in the literature (70 GPa, [36]), indicated by the horizontal line. Very good agreement in the *E* value was obtained using the calibrated diamond area function (DAF).

Nanoindentation results are discussed for all specimens exhibiting a close moisture content of 8 + 1%. Therefore, it is expected that the comparison of local mechanical properties does not rely on overall water content effect. Fig. 6a shows examples of the indentation response force-depth at three different positions, for starch (S) and protein (PPI) free of starchy matrix, and starch/protein interphase of L_SP1/1 composite.

The corresponding position of each indentation curve was identified using the optical microscopy images of imprints generated upon indentation (Supplementary materials, Fig.A1). Indents could be

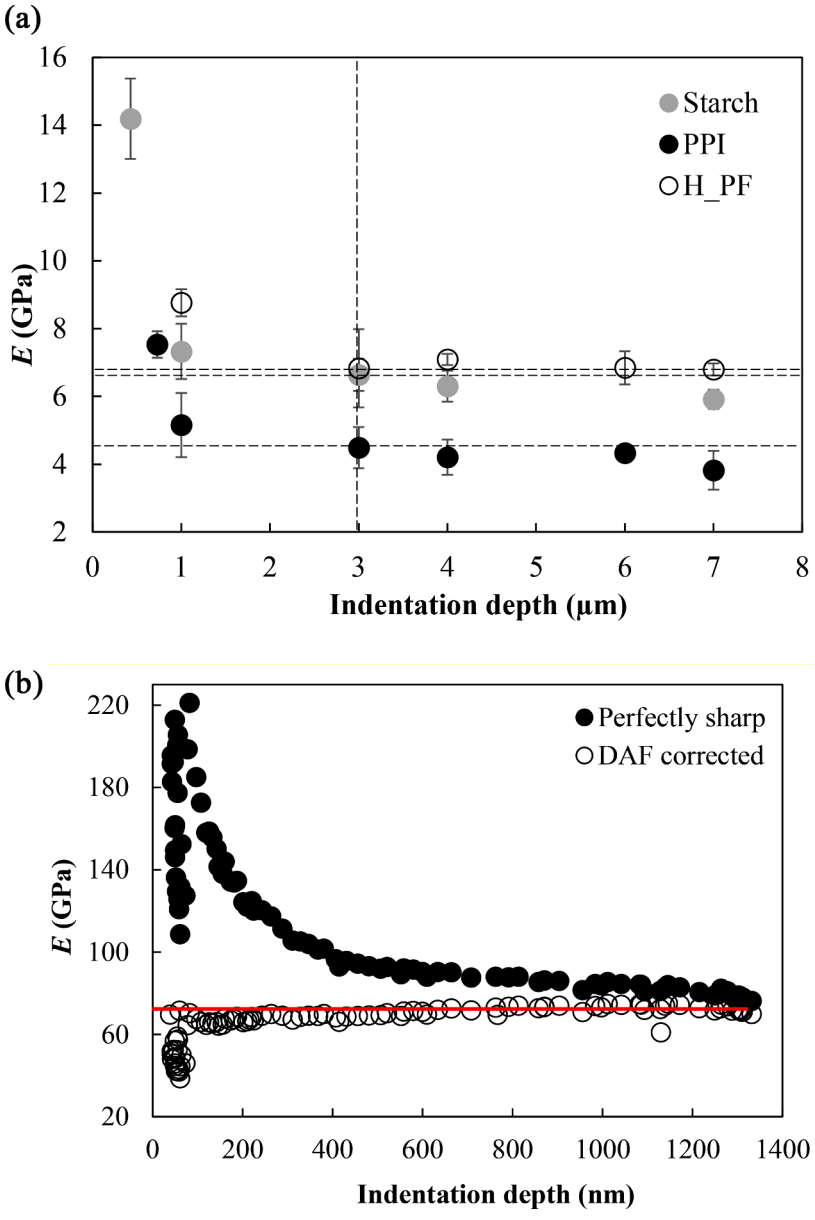

Fig. 5. Variation of Young's modulus (*E*) of extruded pea starch, pea protein isolates (PPI) and H_PF composite with indentation depth. For each sample, *E* was taken as the average from 4 indentations for each depth regardless of the position of imprints. The horizontal dotted lines refer to *E* values obtained at 3 μm depth. **(b)** Young's modulus (*E*) of reference material (fused silica) computed using two hypotheses: perfectly sharp tip (●) and diamond area function (DAF) (o). The DAF corrected *E* is close to the literature value (red line) at indentation depths >50 nm.

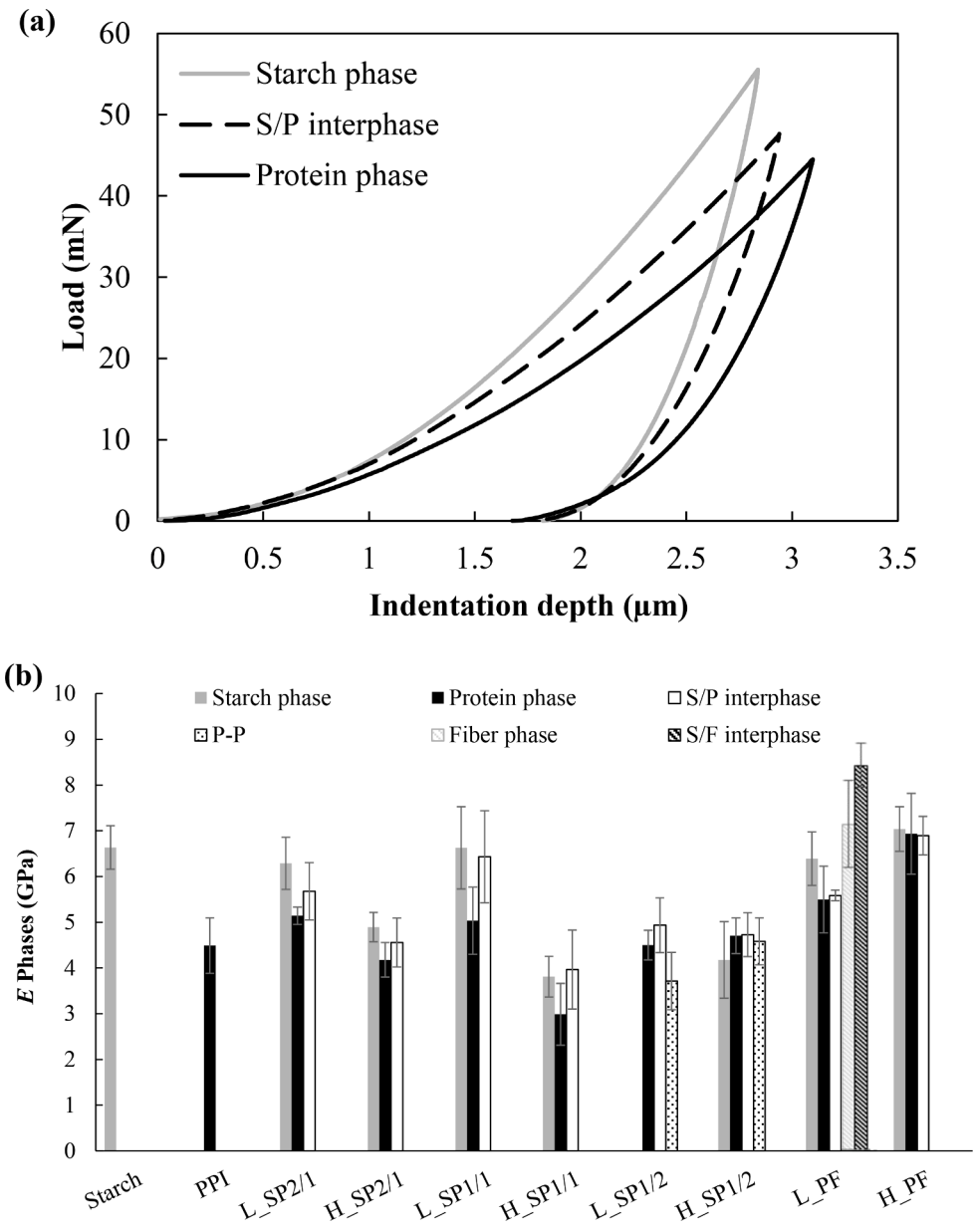

Fig. 6. (a) Typical nanoindentation curves obtained at starch and protein phases, and starch/protein (S/P) interphase for sample L_SP1/1. (b) Young's modulus (*E*) of different phases in composites: starch, protein, fibre, starch/protein (S/P) and starch/fibre (S/F) interphases, and at contact between protein particles (P-P). The property of fibrous phase and S/F interphase is available only for pea flour composite L_PF. The modulus *E* of starch phase is not available for composite L_SP1/2 because no indentation curve could be obtained for this phase (no starch phase could be detected in the indentation grid, see appendix, Fig.A1).

situated at the starch, protein and fibre phases, and at the starch/protein (S/P) and starch/fibre (S/F) interphases. The interphase properties consider the contribution of both phases in addition to the interface layer.

An average *E* was measured for each phase and interphase in pea composites, in addition to an average *E* of extruded pure starch S and PPI samples (Fig. 6b). Imprints at contact between protein particles were observed on SP 1/2 composites having the highest protein content (61% db). Fibre phase and S/F interphase were detected on the PF based composite L_PF (see Supplementary materials, Fig.A1). All indentation grids showed imprints on the starch and protein phases, and S/P interphase except for L_SP1/2, for which no imprints could be observed on the starch phase.

The measured *E* for starch and PPI samples were 6.6 ± 0.5 GPa and 4.5 ± 0.6 GPa, respectively (Fig. 6b). The *E* of composites are in the range of 3–6.9 GPa for protein phase, 4–6.9 GPa for S/P interphase and 4.2–7 GPa for starch matrix. These values are in the same order of magnitude as *E* values obtained by nanoindentation on other starch/protein composites, for example those made from extruded corn flour and starch-zein blends: 4.4 ± 0.2 GPa, 4.6 ± 0.2 GPa and 3.7 ± 0.2 GPa for the starchy matrix, zein (maize protein considered as filler) and the interphase, respectively [26].

At this point it should be noted that the protein stiffness measurements could be influenced by deformation of the starch (and vice-versa). Yan et al. (2012) considered this problem in detail and they determined a critical particle size, below which the measured stiffness exceeds the true stiffness by more than 10%. For a 3 µm indent into a soft particle within a hard matrix, this critical size was ~25–50 µm, depending on the ratio of the particle yield strength to matrix stiffness. So this effect can be discarded for SP blends composites because most of the particles indented here are significantly wider than 30–60 µm, except for PF composites.

The fibre phase and starch/fibre interphase exhibited the highest values of *E*, 7 ± 1 GPa and 8 ± 0.5 GPa, respectively (Fig. 6b). If not to be attributed to the overestimation of stiffness due to low particle size, this result can be explained by the well-known reinforcement effect of fibres used to give strength, stiffness and toughness to the biocomposite structure [12, 21, 37, 38]. Using the nanoindentation test,

Rodriguez-Castellano et al. (2015) demonstrated that adding cellulose fibre to starch-gelatine matrix increases the modulus of biocomposites from 1.1 GPa to 2.4 GPa. This result was attributed to a good adhesion and chemical compatibility between cellulose and starch/gelatine matrix, promoted during composite processing by extrusion. Bourmaud and Baley [37] also suggested that the nano-mechanical behaviour of biocomposites reinforced with plant fibres depends on the morphology and mechanical properties of the fibre. More recently, Skamiotis et al. (2018) explained that the increase of toughness of extruded starch, up to 21%, with addition of short cellulose fibres (2.5% w/w) is due to the synergistic effect of fibre-matrix de-bonding and fibre breakage mechanisms at the crack tip.

Overall, we can conclude from Fig. 6b that pea composites presented significant differences between local mechanical properties associated to each phase and interphase (ANOVA, $p<0.5$, at 5% confidence level, Supplementary materials Table A2). Thus, this study enables the quantification of the heterogeneity of local mechanical properties associated with protein content and morphological features as determined by CSLM. Also, it can be stated that the quality of the composite is improved with high intrinsic phase properties because the composite stiffness would benefit at the same time from the positive contribution of the intrinsic properties (starch stiffness) as well as the interphase ones (Fig. 6). In this regard, a higher content of starch is thus a leverage to achieve even higher composite quality. However, this statement does not necessarily mean that the interface quality continuously increases knowing that the interphase properties is a mix between phase and interface performance. Fig. 6 suggests that the interface does not bring significant weakness to the overall composite quality because the interphase moduli lying, in most cases, within the range of the starch and protein properties.

4. Discussion

4.1. Effect of protein content and morphological features

The modulus of a pure amorphous starch sample is equal to or higher than that of starch phase in pea composites, whereas *E* of PPI is equal or lower than those of protein phase in composites, except for the

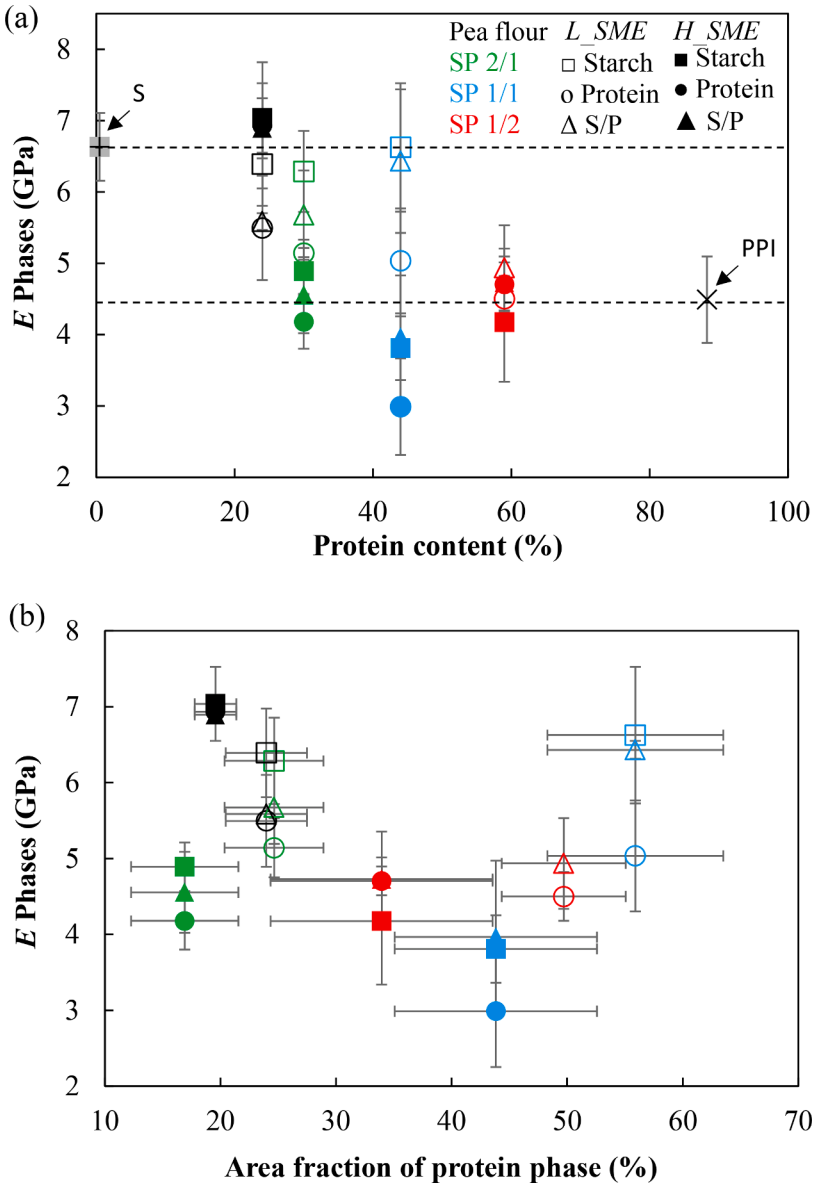

Fig. 7. Young's modulus (*E*) of starch (square symbols) and protein (circle symbols) phases and starch/protein interphase (triangles symbols) as a function of: (a) protein content and (b) area fraction of protein phase (*AFP*) determined by CSLM images analysis. Empty and full symbols refer to samples extruded at low and high *SME*, respectively. Colors refer to the composite's formulation: black for pea flour, green for SP2/1, blue for SP 1/1 and red for SP 1/2. The *E* of extruded starch ((⊕)) and PPI (×) were also shown in (a) by horizontal dotted lines. *E* of starch phase is not available for composite L_SP1/2 (Low *SME*, 60% protein content).

composite H_SP1/1, which exhibits the lowest values of phase and interphase modulus (Fig. 7a).

The variation of *E* of phases and interphase as a function of protein content (%) indicates a large variability across protein contents, which is important when designing the biocomposites (Fig. 7a). As seen from the overlapping of error bars, the difference of *E* values between phases for SP1/2 based composites extruded at high and low *SME*, was not significant ($p>0.5$, ANOVA, Supplementary material Table A2).

However, for other composites, significant differences of *E* values were obtained between the two levels of *SME,* for the same composition ($p<0.5$), likely because of biopolymers structural changes (starch melting, protein aggregation) during extrusion at different levels of *SME* [29]. Indeed, these changes may involve biopolymers degradation under heat and shear as commonly reported by early studies on extrusion [39]. In addition, significantly higher values of *E* for starch phase were found in comparison to protein phase ($p< 0.5$) for composites SP 2/1 (14–19%), L_PF (14%) and SP 1/1 (21–24%). Fig. 7a exabits the variation of Young's modulus as a function of the area fraction of protein phase, where the symbols used in the caption are the same as those reported in Fig. 4a. This figure shows the *E* value of every phase of the composites extruded at high *SME* decreased with protein addition at level less than 50%.

Since the variations of AFP was not directly linked to protein content, the variations of *E* values of phases and interphase with AFP displayed a distinct trend (Fig. 7b), regardless of the *SME* level. *E* decreases until AFP is about 45% and then increases until an *AFP* of approximately 60%. Since H_SP1/1, which exhibits lowest *E* values, had highest interface index value I_i, this result could be explained by a larger number of voids at the interface, as suggested in former studies [33, 34].

4.2. Starch and protein phases versus S/P interphase

Overall, the mechanical properties of starch and protein phases strongly correlated with interphase *E* ($R^2 = 0.8–0.9$) (Fig. 8). The higher the elasticity of the interphase, the higher the elasticity of the surrounding biopolymers. Rjafiallah et al. [13] suggested that the variation of interphase properties could be due to different equilibrium values of MC between starch and protein phases, with an abrupt change in the profile of water content crossing the interface. Indeed, Fig. 8 showed that the *E* value of interphase is equal or lower than that of starch phase, and equal or higher than that of protein phase for almost all samples (except for the SP1/2 composite). This result confirms that the mechanical properties of the protein phase are lower than those of the starch phase for composites having protein content less than approximately 50% (db) protein content (see Fig 7a). Conversely, it underlines the contribution of the starch phase in increasing the interphase properties.

4.3. Validity of local properties at macroscopic scale

The validity of local properties obtained from nanoindentation experiments is discussed hereafter with regards to macroscopic three-point bending results obtained on the same starch-protein composites. Preliminary mechanical testing of pea composites using three-point bending test at different displacement rates (50–200 mm/min, MC 12% wb, 20 °C) showed that the mechanical properties of pea composites t are time independent and can be treated as elastic-plastic materials. The three-point bending test of composites revealed that PF composites and PPI exhibited brittle behaviour with the rupture of specimens in the elastic domain. SP blends composites and starch were less brittle because their rupture took place beyond the initial linear region (Fig. 9).

PFcomposites presented the highest values of engineering flexural moduli (Fig. 10). This may be due to the reinforcing effect of the fibre phase (7 ± 1 GPa) in PF samples as showed by the fibre phase nanonindentation results (see Supplementary materials, Fig.A1). Therefore, adding fibres in SP blends could enhance their mechanical properties. For example, by means of a simple mixture law, the fibre content required to achieve the highest modulus can be calculated for the considered blends. Indeed, in order to achieve the highest modulus for PF, which is 3.1 GPa (PF_H), the amount of fibre additions are 1–2% for SP 2/1, 2–4% for SP 1/1 and 2–9% for SP 1/2. The variations of engineering flexural modulus (*E*) with respect to the I_iI show that, despite a large dispersion of these values, a positive correlation can be obtained ($R^2 = 0.54$, Fig. 10), except for the PF_L sample (at I_i 3.2), due to a lower continuity of the starch phase of its morphology (Fig. 3). The large dispersion of points does not allow highlighting a strong correlation. These results confirm that the mechanical properties of pea products are not exclusively dependent on their morphology; their local mechanical properties must have a substantial effect.

Regarding the comparisons between the local and global mechanical testing, local behaviour suggests that at the same volume fraction of

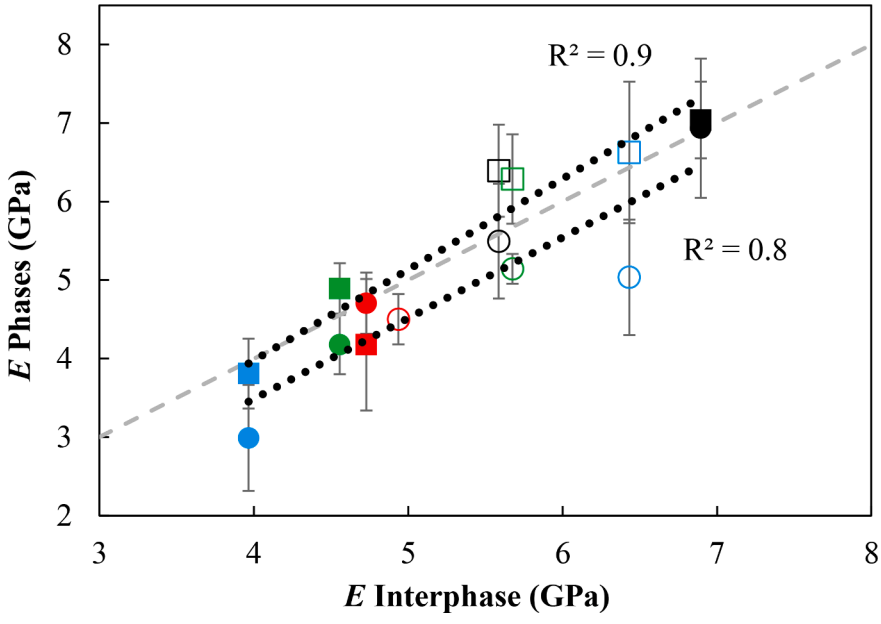

Fig. 8. Variation of Young's modulus (*E*) of starch (square symbols) and protein (circle symbols) phases with those of starch/protein interphase. Empty and full symbols refer to samples extruded at low and high *SME,* respectively. *E* in starch phase was not measured for L_SP1/2 (Low SME, 60% protein content). The black dotted lines represent the data fitting according to the functions $y = 1.2\,x - 0.6$ ($R^2 = 0.9$) for starch phase and $y = x - 0.6$ ($R^2 = 0.8$) for protein phase, and the grey one corresponds to $Y = X$ line.

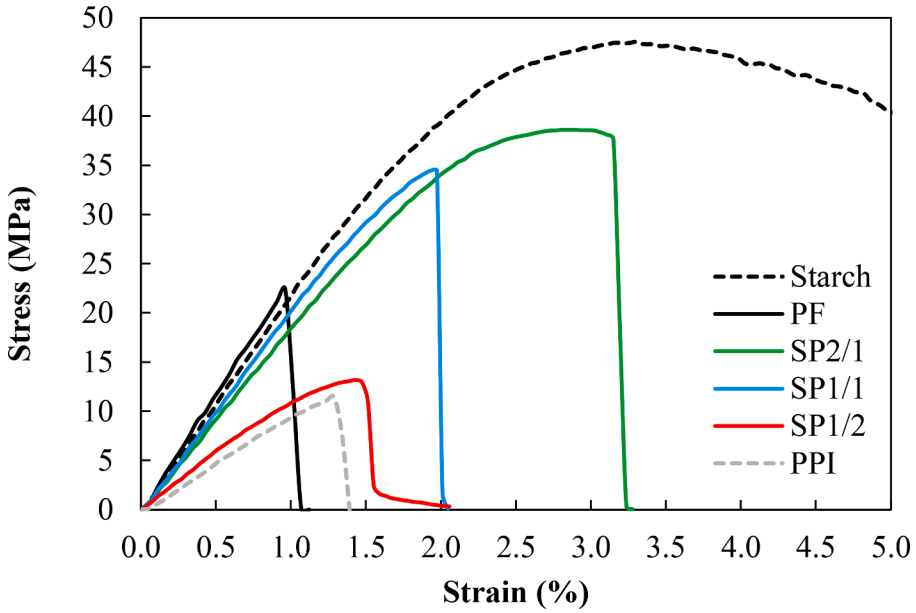

Fig. 9. Examples of flexural response obtained for pea-based composites (20 °C, *MC*12 ± 0.5% wb).

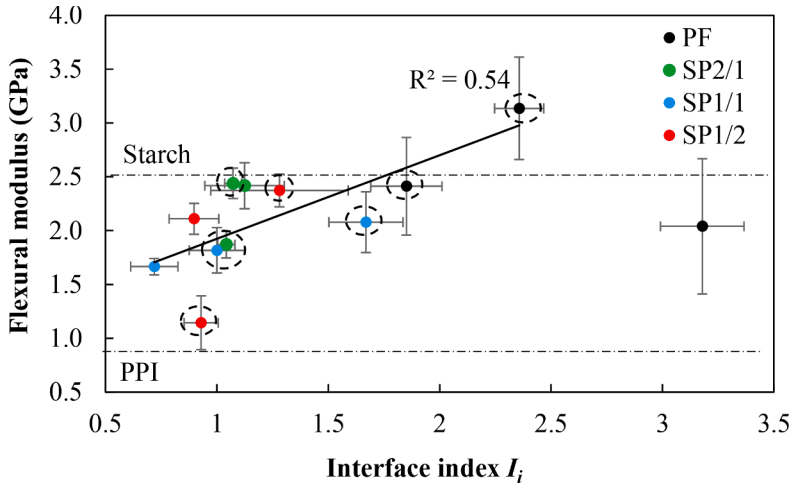

Fig. 10. Engineering flexural modulus of studied composites as a function of interface index. The horizontal dotted lines correspond to the mechanical properties of pure constituents (PPI, starch). The linear fitting curve has the following equation $E_f = 0.78 \times I_i + 1.1$ for (c, excluding the highest point). The dotted circles correspond to the samples selected for the local mechanical test.

proteins, differences in elasticity behaviour can be observed depending on the microstructural arrangements. This means not only the macroscopic behaviour is affected by the quantity of interfaces (under weak interface hypothesis), but also interfacial stiffness as well (Fig. 8, 10). At the same temperature (20 °C), *E* values of pea composites obtained by nanoindentation test were about three times higher than those obtained using macroscopic three-point bending test of ribbon specimens (40 × 10 × 1 mm^3), which were in the range of 2–3.1 GPa (ANOVA, $p<0.5$, at 5% confidence level). This difference is explained by a nanoindentation modulus derived from the unloading phase whereas the modulus from the three-point bending test is derived from the loading phase, where accuracy in measuring elastic deformation may be compromised. Moreover, knowing that amorphous starch mechanical properties depend on moisture [40], it could also be partly due to a different MC, which was 12±1% for macroscopic testing (see [30]) vs 8 ± 1%, here, resulting from sample drying during preparation for nanoindentation experiments.

5. Conclusions

This study shows that the interface in pea-based starch-protein composites plays an important role in controlling the mechanical properties of the composite. Indeed, engineering flexural modulus dependence on interface index materialises at the microstructural scale by a positive correlation between phase and interphase stiffness. This study concludes, however, on different magnitudes of phase and interphase evidenced from local mechanical testing. The interphase modulus ranges between that of the protein (3–6.9 GPa) and the starch phases (4.2–7 GPa). The composites with 61% (db) of protein content (SP blend 1/2) do not display any significant difference between phases and interphase modulus. Up to a protein content of approximately 50% db, the local mechanical properties of the composites depend on the biopolymers' transformation during extrusion and the contrast in phase Young's moduli is significant. In addition, a protein content up to 50% db in the composite induces low local properties, especially for high transformation levels. Furthermore, no protein reinforcing effect is

explained by a low Young's modulus of protein, presence of interfacial voids and likely the incompatibility between starch and protein phases. Finally, the presence of fibre in pea flour enhances the mechanical properties of pea flour-based composites. Then, adding fibres on SP blends can be an alternative to improve their global mechanical properties. However, increased fragility of composites by adding proteins can be considered advantageous for chewing easiness of protein-fortified foods and nutraceutical release performance in biomedical implants. Both nanoindentation and global testing results highlight the same tendency with respect to the morphological features. However, global mechanical testing still provides the lowest magnitudes for the same formulation and morphological feature (I_i). These results confirm the important effect of their intrinsic mechanical properties. In a future work, these results will provide a framework for finite element modelling (FEM) to predict the effective mechanical properties of starch-protein composites from their morphology.

Declaration of Competing Interest

The authors declare that they have no known competing financial interests or personal relationships that could have appeared to influence the work reported in this paper.

Acknowledgements

The authors are grateful to Ruth Brooker from mechanical department at Imperial College, to Anne-Laure Reguerre & Jean-Eudes Maigret from INRAE for technical assistance. This work was partly supported by COST Action (CA15118 - Mathematical and Computer Science Methods for Food Science and Industry).

Supplementary materials

Supplementary material associated with this article can be found, in the online version, at doi:10.1016/j.jcomc.2022.100272.

References

[1] Mohanty A.K., Misra M., Drzal L.T.J. Polym. Environ.. 2002; 10(1/2):19–26.
[2] T. Jiang, Q. Duan, J. Zhu, H. Liu, L. Yu, Starch-based biodegradable materials: challenges and opportunities, Advanced Industrial and Engineering Polymer Research 3 (1) (2020) 8–18.
[3] A.P. Abbott, T.Z. Abolibda, S.J. Davis, F. Emmerling, D. Lourdin, E. Leroy, et al., Glycol based plasticisers for salt modified starch, RSC Adv. 4 (76) (2014) 40421–40427.
[4] M. Gáspár, Z. Benkő, G. Dogossy, K. Réczey, T. Czigány, Reducing water absorption in compostable starch-based plastics, Polym. Degrad. Stab. 90 (3) (2005) 563–569.
[5] Y.X. Xu, K.M. Kim, M.A. Hanna, D. Nag, Chitosan–starch composite film: preparation and characterization, Ind. Crops Prod. 21 (2) (2005) 185–192.
[6] N. A, X. Li, X. Zhu, Y. Xiao, J Che, Starch/polylactide sustainable composites: interface tailoring with graphene oxide, Compos. Part A 69 (2015) 247–254.
[7] J. George, L.B. Azad, A.M. Poulose, Y. An, A.K. Sarmah, Nano-mechanical behaviour of biochar-starch polymer composite: investigation through advanced dynamic atomic force microscopy, Compos. Part A 124 (2019), 105486.
[8] R. Moriana, F. Vilaplana, S. Karlsson, A. Ribes-Greus, Improved thermo-mechanical properties by the addition of natural fibres in starch-based sustainable biocomposites, Compos. Part A 42 (1) (2011) 30–40.
[9] A. Hamma, M. Kaci, Z.A. Mohd Ishak, A Pegoretti, Starch-grafted-polypropylene/kenaf fibres composites. Part 1: mechanical performances and viscoelastic behaviour, Compos. Part A 56 (2014) 328–335.
[10] T. Gurunathan, S. Mohanty, S.K. Nayak, A review of the recent developments in biocomposites based on natural fibres and their application perspectives, Composites, Part A 77 (2015) 1–25.
[11] Y. Lu, L. Weng, X. Cao, Biocomposites of Plasticized Starch Reinforced with Cellulose Crystallites from Cottonseed Linter, Macromol. Biosci. 5 (11) (2005) 1101–1107.
[12] W. Rodríguez-Castellanos, F.J. Flores-Ruiz, F. Martínez-Bustos, F. Chiñas-Castillo, F.J. Espinoza-Beltrán, Nanomechanical properties and thermal stability of recycled cellulose reinforced starch-gelatin polymer composite, J. Appl. Polym. Sci. 132 (14) (2015) n/a-n/a.
[13] S. Rjafiallah, S. Guessasma, D. Lourdin, Effective properties of biopolymer composites: a three-phase finite element model, Compos. Part A 40 (2) (2009) 130–136.
[14] H. Kargarzadeh, N. Johar, I. Ahmad, Starch biocomposite film reinforced by multiscale rice husk fiber, Compos. Sci. Technol. 151 (2017) 147–155.
[15] Y. Zhang, L. Cui, X. Che, H. Zhang, N. Shi, C. Li, et al., Zein-based films and their usage for controlled delivery: origin, classes and current landscape, J. Controlled Release 206 (2015) 206–219.
[16] E.J. Bealer, S. Onissema-Karimu, A. Rivera-Galletti, M. Francis, J. Wilkowski, D. Salas-de la Cruz, et al., Protein–Polysaccharide Composite Materials: fabrication and Applications, Polymers (Basel) 12 (2) (2020) 464.
[17] L. Day, B.G. Swanson, Functionality of protein-fortified extrudates, Compr. Rev. Food Sci. Food Saf. 12 (5) (2013) 546–564.
[18] S. Guessasma, L. Chaunier, G. Della Valle, D Lourdin, Mechanical modelling of cereal solid foods, Trends Food Sci. Technol. 22 (4) (2011) 142–153.
[19] N. Logié, G. Della Valle, A. Rolland-Sabaté, N. Descamps, J Soulestin, How does temperature govern mechanisms of starch changes during extrusion? Carbohydr. Polym. 184 (2018) 57–65.
[20] W.C. Oliver, G.M. Pharr, An improved technique for determining hardness and elastic modulus using load and displacement sensing indentation experiments, J. Mater. Res. 7 (6) (2011) 1564–1583.
[21] S. Cárdenas-Pérez, J.J. Chanona-Pérez, J.V. Méndez-Méndez, G. Calderón-Domínguez, R. López-Santiago, I Arzate-Vázquez, Nanoindentation study on apple tissue and isolated cells by atomic force microscopy, image and fractal analysis, Innovative Food Sci. Emerg. Technol. 34 (2016) 234–242.
[22] O. Das, A.K. Sarmah, D. Bhattacharyya, Nanoindentation assisted analysis of biochar added biocomposites, Compos. B. Eng. 91 (2016) 219–227.
[23] O. Das, M.S. Hedenqvist, C. Prakash, R.J.T. Lin, Nanoindentation and flammability characterisation of five rice husk biomasses for biocomposites applications, Compos. Part A 125 (2019).
[24] O. Das, T. Loho, A. Capezza, I. Lemrhari, M. Hedenqvist, A Novel Way of Adhering PET onto Protein (Wheat Gluten) Plastics to Impart Water Resistance, Coatings 8 (11) (2018).
[25] S.-.H. Lee, S. Wang, G.M. Pharr, H. Xu, Evaluation of interphase properties in a cellulose fiber-reinforced polypropylene composite by nanoindentation and finite element analysis, Compos. Part A 38 (6) (2007) 1517–1524.
[26] S. Guessasma, W. Zhang, J. Zhu, Local mechanical behavior mapping of a biopolymer blend using nanoindentation, finite element computation, and simplex optimization strategy, J. Appl. Polym. Sci. 134 (24) (2017).
[27] S. Guessasma, M. Sehaki, D. Lourdin, A. Bourmaud, Viscoelasticity properties of biopolymer composite materials determined using finite element calculation and nanoindentation, Comput. Mater. Sci. 44 (2) (2008) 371–377.
[28] S. Rjafiallah, N. Benseddiq, S. Guessasma, Effect of interface properties on the effective properties of biopolymer composite materials. Einfluss der Grenzflächeneigenschaften auf die effektiven Eigenschaften von Biopolymer-Verbundwerkstoffen, Materwiss Werksttech 41 (5) (2010) 265–269.
[29] M. Kristiawan, V. Micard, P. Maladira, C. Alchamieh, J.E. Maigret, A.L. Réguerre, et al., Multi-scale structural changes of starch and proteins during pea flour extrusion, Food Res. Int. 108 (2018) 203–215.
[30] I. Jebalia, J.E. Maigret, A.L. Réguerre, B. Novales, S. Guessasma, D. Lourdin, et al., Morphology and mechanical behaviour of pea-based starch-protein composites obtained by extrusion, Carbohydr. Polym. 223 (2019), 115086.
[31] A.K. Jain, Data clustering: 50 years beyond K-means, Pattern Recognit. Lett. 31 (8) (2010) 651–666.
[32] Q. Dehaine, L.O Filippov, Modelling heavy and gangue mineral size recovery curves using the spiral concentration of heavy minerals from kaolin residues, Powder Technol. 292 (2016) 331–341.
[33] H. Chanvrier, P. Colonna, G. Della Valle, D Lourdin, Structure and mechanical behaviour of corn flour and starch–zein based materials in the glassy state, Carbohydr. Polym. 59 (1) (2005) 109–119.
[34] E. Habeych, B. Dekkers, A.J. van der Goot, R. Boom, Starch–zein blends formed by shear flow, Chem. Eng. Sci. 63 (21) (2008) 5229–5238.
[35] M.E. Camire, Protein functionality modification by extrusion cooking, J. Am. Oil Chem.' Soc. 68 (3) (1991) 200–205.
[36] X. Li, B. Bhushan, A review of nanoindentation continuous stiffness measurement technique and its applications, Mater. Charact. 48 (1) (2002) 11–36.
[37] A. Bourmaud, C. Baley, Nanoindentation contribution to mechanical characterization of vegetal fibers, Compos. Part B. Eng. 43 (7) (2012) 2861–2866.
[38] C.G. Skamniotis, Y. Patel, M. Elliott, M.N. Charalambides, Toughening and stiffening of starch food extrudates through the addition of cellulose fibres and minerals, Food Hydrocoll. 84 (2018) 515–528.
[39] Mercier C., P. Linko, and J.M. Harper. Extrusion cooking Amer Assn of Cereal Chemists; 1989.
[40] M. Kristiawan, L. Chaunier, G. Della Valle, D. Lourdin, S Guessasma, Linear viscoelastic properties of extruded amorphous potato starch as a function of temperature and moisture content, Rheol. Acta 55 (7) (2016) 597–611.